# A 12-years long (2010-2021) hydrological and biogeochemical dataset in the Sicily Channel (Mediterranean Sea)

Francesco Placenti[1], Marco Torri[2*], Katrin Schroeder[3], Mireno Borghini[4], Gabriella Cerrati[5], Angela Cuttitta[2], Vincenzo Tancredi[1], Carmelo Buscaino[1], Bernardo Patti[6]

[1]Consiglio Nazionale delle Ricerche - Istituto per lo studio degli impatti Antropici e Sostenibilità in ambiente marino (CNR-IAS), Campobello di Mazara (TP), Italy.
[2]Consiglio Nazionale delle Ricerche – Istituto di Studi sul Mediterraneo (CNR-ISMed), Palermo, Italy.
[3]Consiglio Nazionale delle Ricerche – Istituto di Scienze Marine (CNR-ISMAR), Venice, Italy.
[4]Consiglio Nazionale delle Ricerche – Istituto di Scienze Marine (CNR-ISMAR), La Spezia, Italy
[5]ENEA – Infrastrutture e Servizi – Servizio e Gestioni Centro Santa Teresa (ISER-STE), Santa Teresa, La Spezia, Italy;
[6]Consiglio Nazionale delle Ricerche - Istituto per lo studio degli impatti Antropici e Sostenibilità in ambiente marino (CNR-IAS), Palermo, Italy.

*Corresponding author: marco.torri@cnr.it

**ABSTRACT**

1   The data set presented here consists of 273 Conductivity-Temperature-Depth (CTD) stations, as well

2   as 2034 sampled data points in the water column, where dissolved inorganic nutrients have been

3   measured, that were collected during 12 summer oceanographic cruises (BANSIC series) in the Sicily

4   Channel (Central Mediterranean Sea), between 2010 and 2021. The quality of the CTD dataset is

5   ensured by regular sensor calibrations, an accurate control process adopted during the acquisition,

6   processing and post-processing phases. The quality of the biogeochemical dataset is ensured by the

7   adoption to best-practices analytical and sampling methods. This data collection fills up a gap of

8   information in the Sicily Channel, i.e. a key area where complex water mass exchange processes

9   involve the transfer of physical and biogeochemical properties between the Eastern and the

10   Western Mediterranean. The available dataset will be useful to evaluate the long-term variability

11   on a wide spatial scale, supporting studies on the evolution of the Mediterranean circulation and its

12   peculiar biogeochemistry, as well as on the physical and biogeochemical modeling of this area.

13

14   **INTRODUCTION**

15   The thermohaline circulation in the Mediterranean Sea (MS) is anti-estuarine and is driven by the

16   negative freshwater budget and the net heat loss over the whole basin. The Mediterranean

17   thermohaline circulation drives the transport of water masses and biogeochemical elements in the

different basins (eastern and western) and, via the Strait of Gibraltar, controls the exchanges with the Atlantic Ocean (The MerMex Group, 2011).

The Sicily Channel (SC), due to its particular bathymetric structure and geographic position, also plays a key role in modulating the eastward transport of the fresher and superficial Atlantic Water (AW) and the underlying westward transport of the salty Intermediate Water (IW) which forms in the Eastern Mediterranean, called Levantine Intermediate Water (LIW) or Cretan Intermediate Water (CIW), depending on the specific formation location (Levantine or Cretan Sea) (Schroeder et al., 2017). From its formation area IW spreads westward into the Ionian Sea (IS), with a significant flow northward towards the Adriatic Sea, where it constitutes an important preconditioning agent for the formation of the Adriatic Deep Water (which forms the bulk of the Eastern Mediterranean Deep Water, e.g. Gačić et al., 2013). When reaching the Western Mediterranean, and in particular its northern part, the IW preconditions the water column also there and makes it prone to the formation of Western Mediterranean Deep Water (e.g., Roether et al., 1996). Although the area of the SC is limited at the east and west by two relatively shallow sills (max depths of 350 m and 550 m, respectively), in its central part the bottom depth can reach 1700 m. It is in this deep central trench where e.g., Gasparini et al. (2005) and others studied the evolution of the upper part of the Eastern Mediterranean Deep Water (or transitional Eastern Mediterranean Deep Water) over time, being able to cross the SC and reach the Tyrrhenian Sea along with the IW flow. Several authors, analyzing long time series of temperature and salinity of the deeper waters of the SC, have highlighted a general positive trend albeit characterized by phases of accelerations and multiannual peaks and fluctuations (Gasparini et al., 2005; Gačić et al., 2013; Bonanno et al., 2014; Ben Ismail et al., 2014; Schroeder et al., 2017; Placenti et al., 2022). Furthermore, these trends are significantly faster than those reported for the global ocean intermediate layer (Borghini et al., 2014; Schroeder et al., 2017). In fact, the semi-enclosed nature of the MS, together with its smaller inertia due to the relative short residence time of its water masses, makes it more sensitive to natural variations in fluxes (between, e.g., the air and sea, freshwater and the sea) and water flows, identifying it as a ''hotspot'' for climate change. Consequently, MS is expected to experience environmental impacts that are considerably greater than those in many other places around the world (The MerMex Group, 2011). As regards the peaks, trends and multiannual fluctuations of temperature and salinity observed in the deeper water of the SC, they are probably ascribable to different processes acting at different spatial and temporal scales, such as the passage of the signature of the Eastern Mediterranean Transient (EMT) (Gasparini et al., 2005), the alternation of circulation phases

50  (cyclonic-anticyclonic) of the Northern Ionian Gyre (NIG) (Gačić et al., 2013; Bonanno et al., 2014;

51  Placenti et al., 2022) and the effects related to warming of  the Eastern Mediterranean (Schroeder

52  et al. al., 2017, 2019).

53  The anti-estuarine circulation, jointly to the superposition of different time scales of variability,

54  intense wintertime atmospheric forcings, NIG reversals and EMT, act also on the distribution of

55  biogeochemical elements (e.g., inorganic nutrients) and productivity of the MS. The very low

56  productivity of the MS is therefore mainly linked both to the anti-estuarine circulation (Krom et al.,

57  2010) and to the chemical speciation of the dissolved P and N. They in fact reflect a switch from less

58  bioavailable chemical forms of P and N entering the Mediterranean Sea to more bioavailable forms

59  leaving it (Powley et al., 2017). Moreover, the export of nutrients through the IW causes the deep

60  waters of the Eastern Mediterranean Sea to be more nutrient depleted than deep water in all other

61  parts of the global ocean (Krom et al., 2005). Another peculiarity still debated is the higher molar

62  $NO_3:PO_4$ ratio in the deeper water of the MS compared to the "classical" world oceans Redfield

63  ratio, indicating a general P-limited regime, which becomes stronger along a west-to-east gradient

64  (Belgacem et al., 2020). In this context, the aim of this paper is to compile a large dataset of

65  hydrological (temperature, salinity and pressure) and biogeochemical (nitrate, phosphate and

66  silicate) properties from *in situ* data collected between 2010 and 2021 in the SC, filling up a gap of

67  information in a key area of the MS, where the exchange between the two basins is taking place.

68  The available dataset is a valuable tool in support to the evaluation of the long-term variability and

69  evolution of the Mediterranean circulation and water masses, and provides also a useful

70  contribution for the implementation of models aimed at describing the physical-chemical processes

71  occurring in this area. The dataset could also be integrated in the recently published climatology of

72  dissolved inorganic nutrients (Belgacem et al., 2020), to expand its geographic domain.

73

74  **DATASET AND METHODS**

75  The hydrological and biogeochemical data collection was carried out as part of an ichthyoplankton

76  monitoring and research program implemented by the Italian National Research Council (CNR). This

77  program was set up with the primary purpose of monitoring the spatio-temporal distribution of the

78  early life stages of European anchovy (*Engraulis encrasicolus*) in the SC and of studying its

79  relationship with the environmental variables, in support to the sustainable exploitation of the

80  population by local fisheries. In this context, since 1998 ichthyoplankton oceanographic surveys

81  based on a common sampling grid have been annually carried out during the summer period in the

82 SC, within the FAO Geographic Sub-Areas (GSAs) 13, 15 and 16. Since 2010, in addition to the meso-

83 zooplancton sampling, water sampling for the quantification of macro-nutrients has been included

84 in the survey work plan in order to better characterize the biogeochemical characteristics of the

85 water column and study the relationships with the biotic component.

86 The dataset presented here results from this sampling effort and assembles information from 12

87 summer oceanographic cruises conducted on board of different research vessels from 2010 to 2021

88 (R/V "Urania" from 2010 to 2014; R/V "Minerva Uno" from 2015 to 2017; R/V "G. Dallaporta" from

89 2018 to 2021). Data were integrated into a dataset consisting of 273 CTD-nutrient stations and 2034

90 data points (Suppl. 1). The stations are arranged along inshore-offshore transects approximately sub

91 perpendicular to the Sicilian coast, aiming at characterizing the oceanographic and biogeochemical

92 features in a key area for the understanding of the complex exchange processes between the

93 Eastern and Western basins (Fig. 1).

*Figure 1. Stations map of the Bansic cruises, carried out in the Sicily Channel or Strait of Sicily from 2010 to 2021: CTD and nutrient stations are indicated by blue (in the general map) and red circles (in the yearly maps). The maps were created using Ocean Data View software (https://odv.awi.de/).*

**Hydrological Data Acquisition**

At all stations, pressure, salinity, and temperature were measured with a CTD (conductivity, temperature, and depth) probe (Sea-Bird Scientific) mod. SBE 911plus and a General Oceanics rosette with 24 Niskin bottles of 12 L capacity. Temperature measurements were performed with a SBE-3/F thermometer, with a resolution of 0.00015 °C/bit at -1 °C or 0.00018 °C/bit at 31 °C, and accuracy of ±0.001 °C. The conductivity measurements were performed with a SBE-4C sensor, with a resolution of 0.00004 S/m and accuracy of 0.0003 S/m, while for the salinity the accuracy is 0.002. The vertical profiles of all parameters were obtained by sampling the signals at 24 Hz, with the CTD/rosette going down at a speed of 1 m/s. The rosette is equipped with a sonar altimeter which intercept the bottom 100-70 meters before getting to it. The altimeter is used just for safety, to avoid the rosette to touch the bottom.

**Inorganic Nutrient Data Collection**

Seawater samples for dissolved inorganic nutrient analysis were collected from the surface to the bottom by means of Niskin bottles. In particular, during the CTD upcast, a variable number of water samples, at selected standard depth, has been considered (surface–25m–50m–75m–100m–150m-200m–300m–400m–500m–600m–700m–800m–900m–1000m–bottom) with slight modifications in the upper layer where significant hydrological variability is typical to occur. All materials used for water sampling on board were earlier conditioned with 10% HCl and rinsed 3 times with ultrapure water. Unfiltered samples were stored on board at –20°C.

**Analytical Methods for Inorganic Nutrients**

For all cruises, nutrient determination (nitrate, silicate, and phosphate) was carried out following standard colorimetric methods of seawater analysis, defined by Grasshoff et al. (1999) and Hansen and Koroleff (1999) adapted to an automated system. Specifically, the determination of phosphate is based on the colorimetric method, in which a blue color is formed by the reaction of phosphate, molybdate ion and antimony ion, followed by reduction with ascorbic acid. The reduced blue phospho-molybdenum complex is read at 880 nm. Inorganic nitrate is reduced to nitrite at pH 8 in a copperized cadmium reduction coil that reacts with an aromatic amine, leading to the final formation of the azo dye measured at 550 nm. Then, the nitrite that is separately determined must be subtracted from the total amount measured to get the nitrate concentration only. The

129 determination of soluble silicates is based on the reduction of a silico-molybdate complex in acid
130 solution to molybdenum blue by ascorbic acid and the absorbance is measured at 820 nm.

131 All the analysis of dissolved inorganic nutrients were carried out immediately after each
132 oceanographic cruise, in the nutrient laboratory of the Institute for the Study of Anthropic Impacts
133 and Sustainability in the Marine Environment (CNR-IAS) of Capo Granitola, using the same analytical
134 instrument and the same scientific staff. The concentration (µmol/l) of nitrate, silicate and
135 phosphate was measured by means of a Sial Autoanalyzer ''QUAATRO''. The detection limits for
136 nitrates, silicates and phosphates were 0.02, 0.01 and 0.006 µmol/l, respectively. Even though the
137 use of the same analytical methods, instruments and scientific staff supports the repeatability and
138 the comparison of the measurements, in order to  further validate  the analytical data, selected
139 seawater samples (sampled in duplicate) have been sent to the nutrient laboratory of nutrients of
140 the Research Center (ENEA) of Santa Teresa (La Spezia), taking advantage on their participation in
141 the framework of the European intercalibration program QUASIMEME (Quality Assurance of
142 Information for Marine Environmental Monitoring in Europe).

143 The differences in concentrations for all parameters analyzed (nitrates, phosphates and silicates)
144 ranged from 3% to 20%. The differences were greater (10-20%) for concentration values close to
145 the instrumental detection limit and smaller (<10%) at high concentrations. This range of differences
146 is perfectly acceptable considering that ENEA uses a previous generation auto-analyser and that the
147 scientific staff was different. However, we would like to point out that, in both nutrient laboratories,
148 the chemical analyzes were carried out using both the same analytical methods and the same types
149 of reagents.

150

151 **Quality check of hydrological and nutrient data**
152 The temperature and salinity of the CTD have been regularly calibrated. During 2 cruises, also
153 redundant temperature and salinity sensors were used. When they were available, the secondary
154 sensors have been used to assess the stability of the primary ones.

155 The temperature and salinity sensors calibrations have been performed before each cruise by CNR
156 technicians at the NATO Centre for Underwater Research (NURC, now Centre for Maritime Research
157 and Experimentation, CMRE) in La Spezia (Italy) until 2016. Between 2017 and 2018 sensors were
158 send to the manufacturer, while since 2019 the calibration is done at the new CNR-ISMAR
159 calibration laboratory in La Spezia (Italy). Table 1 shows a summary of all sensors, their serial
160 numbers and their calibration dates.

*Table 1. Calibration dates and serial numbers of the CTD sensors used during oceanographic cruises.*

| Cruise | Date | Temp 1 | | Cond 1 | | Temp 2 | | Cond 2 | |
|---|---|---|---|---|---|---|---|---|---|
| | | sn | cal. date | sn | cal. date | sn | cal. date | sn | cal. date |
| Bansic 2010 | 25 Jun–14 Jul 2010 | 1368 | May10 | 891 | May10 | | | | |
| Bansic 2011 | 08–26 Jul 2011 | 4440 | Apr11 | 3172 | Apr11 | | | | |
| Bansic 2012 | 04–23 Jul 2012 | 1183 | Nov10 | 923 | Nov10 | | | | |
| Bansic 2013 | 26 Jun–16 Jul 2013 | 2810 | Oct12 | 2483 | Oct12 | | | | |
| Bansic 2014 | 22 Jul–9 Aug 2014 | 4440 | Nov13 | 3172 | Nov13 | | | | |
| Bansic 2015 | 16 Jul–3 Aug 2015 | 5022 | Oct14 | 3485 | Nov14 | | | | |
| Bansic 2016 | 30 Jun–14 Jul 2016 | 5022 | Oct14 | 3485 | Nov14 | | | | |
| Bansic 2017 | 13–29 Jun 2017 | 1183 | Jul16 | 0923 | Jun16 | | | | |
| Bansic 2018 | 07-19 Sep 2018 | 1142 | Aug17 | 2779 | Aug17 | | | | |
| Bansic 2019 | 30 Sep-12 Oct 2019 | 1142 | Aug17 | 2779 | Feb19 | 5038 | May17 | 3484 | Feb19 |
| Bansic 2020 | 16-25 Sep 2020 | 1142 | Jan20 | 2779 | Jan20 | 5038 | Jan20 | 3484 | Jan20 |
| Bansic 2021 | 6-18 Sep 2021 | 1381 | Jun21 | 1048 | Jun21 | | | | |

After their acquisition, CTD data were pre-processed by the SBE Data Processing™ software, in order to (i) convert the raw data (.hex) to engineering units and store them in a text file (.cnv) (ii) run a low-pass filter on the data and smooth high frequency data, (iii) align parameter data in time, relative to pressure (to ensure that calculations of salinity and other parameters are made using measurements from the same parcel of water), (iv) remove conductivity cell thermal mass effects from the measured conductivity, (v) compute derived variables, and to (vi) average data, using averaging intervals based on depth range, and split the file into an upcast and a downcast file. Following the recommendations of the SeaDataNet QC guidelines (SeaDataNet, 2010). The subsequent procedure to assess data quality was based on the following list:

- Check header details (vessel, cruise number, station numbers, date/time, latitude/longitude (start and end), instrument number and type, station depth, cast (up or down)), data type/no. of data points)
- Plot station positions to check not on land
- Check ship speed between stations to look for incorrect position or date/time
- Automatic range checking of each parameter
- Check units of parameters supplied
- Check pressure increasing
- Check no data points below bottom depth
- Plot profiles (individually, in groups, etc)
- Check for spikes
- Check for vertical stability/inversions
- Plot temperature vs. salinity

After the data acquisition, a post-processing control has been applied to the hydrological and nutrient data acquired in the single survey as follow. After an initial visual inspection aimed at removing any spike from the data profiles, an automatic control was carried out in R environment in order to identify potential outliers. In particular, taking into account three layers (0-150 m, 151-500 m and >500 m), potential outliers have been defined as values falling outside the range mean ± 3*standard deviation calculated in the relevant layer. Then, each potential outlier has been visually double-checked within the recorded profiles in order to be validated or eliminated from the dataset. Finally, with the aim at evaluating the consistency of the dataset collected in the 2010-2021 annual surveys and performing a comparative control of the occurring patterns among years, the mean value and the coefficient of variation (CV), i.e., a normalized measure of the dispersion given by the ratio of the standard deviation to the mean, of hydrological and nutrient parameters were calculated separately for each survey and for every identified water mass (Tab. 2). In this context, based on the annual θ-S diagrams (as whole reported in Fig. 2h), three water masses were identified in the study area and schematized below a surface layer of approximately 150 meters thick, variable over the years and occupied mainly by AW, an intermediate layer (200-500 m) mainly occupied by IW and a deeper layer (>500 m) occupied by the upper part of the deep water (DW).


**RESULTS AND DISCUSSION**

An analysis was conducted in order to characterize the spatial-temporal trends emerging in the dataset and compare them with the state of the art concerning the study area. In this framework, the vertical distribution pattern of inorganic nutrients in the water column of the SC highlights low concentration values and high variability (Fig. 2; Tab. 2).
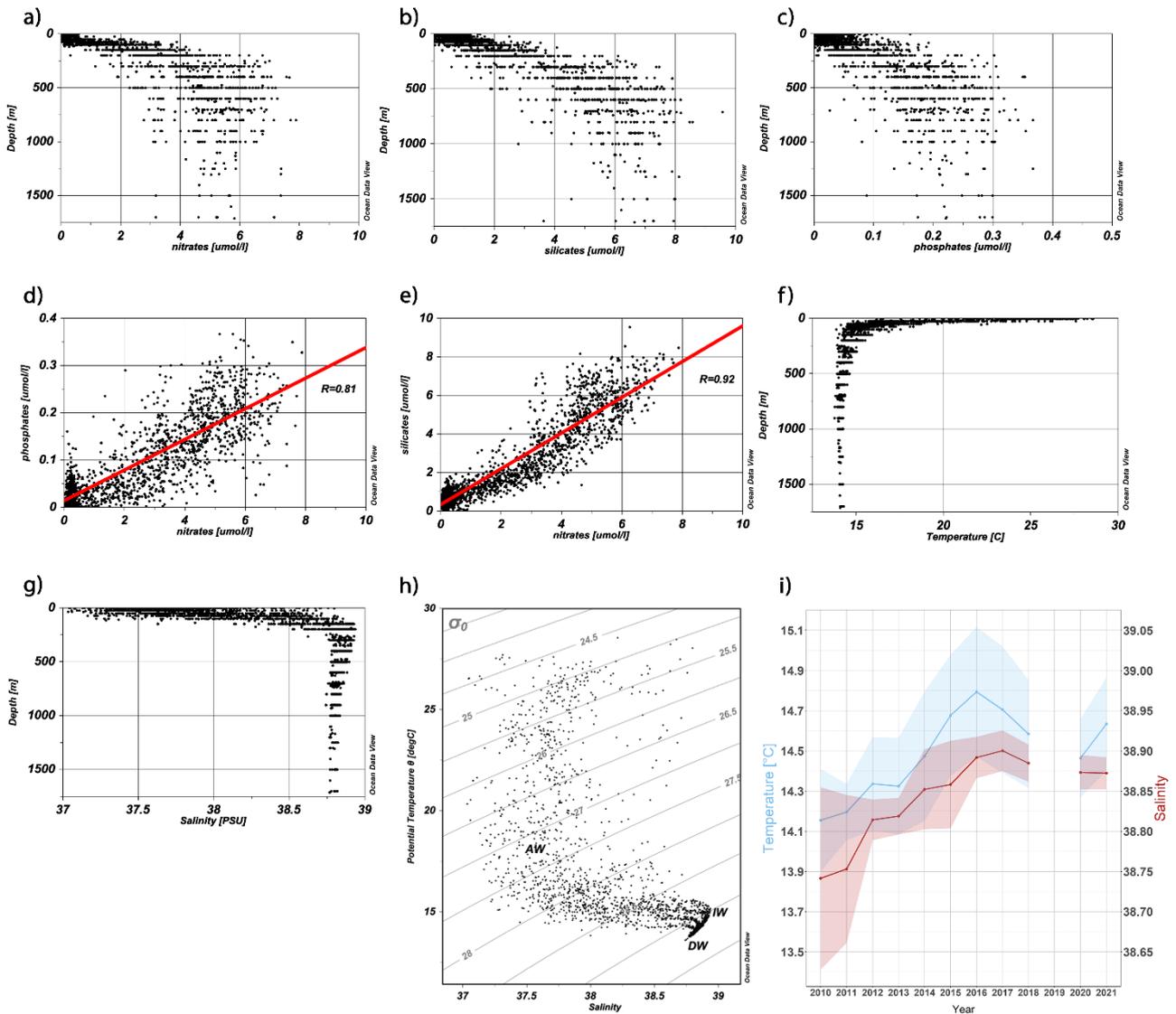
*Figure 2. Plots of data on nutrients concentration at selected standard depths along the water column for a) nitrates, b) silicates, c) phosphates; d) N:P and e) N:Si diagrams and related linear regression lines (in red); f) plots of hydrological data at selected standard depths along the water column for temperature and g) salinity; h)potential temperature vs salinity diagram related to 2010-2021 period (AW for Atlantic Water, IW for Intermediate Water and DW for upper Deep Water) and i) time series of annual average values (2010-2021) of temperature (blue line) and salinity (red line) related to the water sampling depths in the IW (200-500 m). The related colored areas represent the standard deviations.*

In surface waters the concentration values of inorganic nutrients are close to the instrumental detection limits due to the typical consumption of phytoplankton during the summer period occurring in this layer. This usually results in considerably lower values compared to patterns

observed in the underlying layers (Tab. 2). Moreover, the depth layer 0-150m is characterized by a higher CV due to the pronounced dynamism of the exchange processes affecting the marine ecosystem in this upper part of the water column as well as the interaction with terrestrial sources of nutrients. Specifically, the lowest mean nitrate concentration value of 0.302 µmol/l was measured in BANSIC19 survey, characterized by a quite low number of water samples collected from continental shelf stations only (no data of the intermediate layer are available from 2019 survey), while the highest concentration value of 1.027 µmol/l was measured in BANSIC14 survey (Tab. 2). Regarding the phosphates the lowest mean concentration value was 0.030 µmol/l (BANSIC12) and the highest one 0.064 µmol/l (BANSIC13), while for silicates the mean concentration values ranged from a minimum of 0.608 µmol/l (BANSIC15) to a maximum of 1.173 µmol/l (BANSIC10) (Tab. 2). The lower sampling effort carried out in BANSIC19 also corresponds to a lower variation of nitrates and phosphates compared to the other surveys, while the silicates showed more homogeneous patterns among surveys. Specifically, in the superficial layer CV varied between 0.762 (BANSIC19) and 1.566 (BANSIC20) for nitrates, between 0.471 (BANSIC19) and 1.333 (BANSIC21) for phosphates, and finally between 0.433 (BANSIC20) and 0.83 (BANSIC15) for silicates.

The inorganic nutrients are continuously consumed by phytoplankton at the sea surface and regenerated in the mesopelagic layer by bacteria, increasing the nutrient concentrations in the deeper water masses over time (e.g., Belgacem et al., 2020). In this way, the intermediate waters of the SC are characterized by higher nutrient concentration values than the overlying layer and lower variability (Fig. 2a-c and Tab. 2). Specifically, mean concentration values in the intermediate waters ranged from 2.976 µmol/l in BANSIC15 to 5.4 µmol/l in BANSIC11 for nitrates, from 2.589 µmol/l (BANSIC15) to 4.86 µmol/l (BANSIC11) for silicates, and from 0.095 µmol/l in BANSIC18 to 0.204 µmol/l in 2021 for phosphates (Tab. 2).

Regarding the dispersion of the values in this layer, nitrates CV ranged between 0.068 (BANSIC20) and 0.402 (BANSIC15), phosphates CV ranged between 0.171 (BANSIC20) and 0.585 (BANSIC16), and silicates CV ranged between 0.161 (BANSIC20) and 0.528 (BANSIC15) (Tab. 2).

In the trench of the SC, the deep layer (see section >500m-bottom of Tab. 2) is characterized by mean concentration values more homogeneous over years than in the above layers. There, the lowest mean concentration values for nitrates and silicates (4.13 and 4.701 µmol/l) were measured in BANSIC15, while the lowest value for phosphates (0.097 µmol/l) was measured during BANSIC10. The highest mean values of nitrates (5.861 µmol/l), phosphates (0.241 µmol/l) and silicates (6.474 µmol/l) were respectively measured during BANSIC11, BANSIC17-21 and BANSIC13. Similarly, the

deep layer is characterized by the lowest variability in nutrient concentrations. Indeed, the nitrate CV varied between 0.0058 (BANSIC10) and 0.299 (BANSIC21), between 0.07 (BANSIC20) and 0.339 (BANSIC10) for the phosphates and between 0.029 (BANSIC20) and 0.277 (BANSIC15) for the silicates.

The molar ratios of nitrate:phosphate (N:P) and silicate:nitrate (Si:N) in the whole water column of the SC show high correlation coefficients  (R=0.81 and 0.92, respectively) (Fig. 2d,e). Specifically, in the surface layer (0-150m) the mean values of N:P and Si:N over the period 2010-2021 are equal to 18 and 1.4 respectively, which become 31 and 0.9 in the intermediate layer (200-500m) and  29 and 1.1 in the deep layer (500m-bottom), in agreement with Ribera D'Alcalà et al. (2003) and with Placenti et al. (2013; 2022).  Observed N:P values are higher than the classical Redfield ratio (16:1). The high N:P ratio can result from either a decrease in phosphate or an increase in nitrate; however, the reason of this anomaly is still unclear (e.g., Schroeder et al., 2010). Among the various hypotheses, we agree about the possible role of external inputs, together with very limited denitrification (Krom et al., 2010; Huertas et al., 2012; Van Cappellen et al., 2014), in explaining the observed very high $NO_3:PO_4$ ratios in the deeper water (Powley et al., 2017).


*Table 2. Average values of concentration and coefficients of variation (CV) of both physical (temperature and salinity) and chemical (nitrates, phosphates and silicates) parameters in the 12 oceanographic surveys carried out yearly over the period 2010-2021 reported in this paper, by depth layer (superficial 0-150m, intermediate 200-500m and deep >500m-bottom).*

| Cruise name | Sapling date | Research vessel name | Station number | Max. Sampling depth [m] | Sample number | Nitrates mean [umol/l] | Nitrates CV | Phosphates mean [umol/l] | Phosphates CV | Silicates mean [umol/l] | Silicates CV | Temperature mean [°C] | Temperature CV | Salinity mean [psu] | Salinity CV |
|---|---|---|---|---|---|---|---|---|---|---|---|---|---|---|---|
| | | | | | | | | | | | | | | | |
| | | | | | Layer 0-150 m | | | | | | | | | | |
| Bansic10 | 25 June–14 Jul 2010 | Urania | 13 | 700 | 62 | 0.743 | 1.172 | 0.043 | 1.009 | 1.173 | 0.697 | 17.477 | 0.148 | 37.610 | 0.011 |
| Bansic11 | 08–26 Jul 2011 | Urania | 34 | 1130 | 154 | 0.736 | 1.446 | 0.034 | 0.831 | 1.002 | 0.686 | 18.574 | 0.234 | 37.978 | 0.0087 |
| Bansic12 | 04–23 Jul 2012 | Urania | 39 | 1711 | 203 | 0.707 | 1.066 | 0.030 | 0.954 | 1.037 | 0.478 | 17.923 | 0.237 | 38.177 | 0.0117 |
| Bansic13 | 26 June–16 Jul 2013 | Urania | 34 | 1700 | 178 | 0.835 | 1.302 | 0.064 | 0.727 | 1.061 | 0.628 | 17.380 | 0.175 | 37.919 | 0.0094 |
| Bansic14 | 22 Jul–9 Aug 2014 | Urania | 32 | 1700 | 164 | 1.027 | 1.116 | 0.051 | 0.803 | 0.940 | 0.703 | 17.997 | 0.201 | 37.872 | 0.0123 |
| Bansic15 | 16 Jul–3 Aug 2015 | Minerva Uno | 31 | 1700 | 158 | 0.681 | 1.117 | 0.036 | 0.893 | 0.608 | 0.833 | 18.313 | 0.240 | 38.206 | 0.0093 |
| Bansic16 | 30 June–14 Jul 2016 | Minerva Uno | 10 | 1700 | 51 | 0.777 | 1.237 | 0.043 | 0.638 | 0.614 | 0.690 | 17.673 | 0.176 | 37.812 | 0.0135 |
| Bansic17 | 13–29 June 2017 | Minerva Uno | 32 | 1700 | 160 | 0.898 | 1.015 | 0.037 | 1.037 | 1.043 | 0.538 | 17.880 | 0.179 | 37.956 | 0.0125 |
| Bansic18 | 07-19 Sept 2018 | G. Dallaporta | 16 | 700 | 77 | 0.957 | 1.286 | 0.039 | 0.671 | 1.150 | 0.649 | 18.646 | 0.229 | 38.091 | 0.0118 |
| Bansic19 | 30 Sept-12 Oct 2019 | G. Dallaporta | 6 | 72 | 21 | 0.302 | 0.762 | 0.040 | 0.471 | 0.721 | 0.605 | 19.784 | 0.189 | 38.037 | 0.0068 |
| Bansic20 | 16-25 Sept 2020 | G. Dallaporta | 11 | 1000 | 44 | 0.596 | 1.566 | 0.032 | 0.697 | 1.083 | 0.433 | 19.861 | 0.222 | 38.091 | 0.0096 |
| Bansic21 | 6-18 Sept 2021 | G. Dallaporta | 15 | 996 | 67 | 0.577 | 1.449 | 0.073 | 1.333 | 1.087 | 0.526 | 19.623 | 0.222 | 37.822 | 0.0128 |

| | | | | | | Layer 200-500 m | | | | | | | | | |
|---|---|---|---|---|---|---|---|---|---|---|---|---|---|---|---|
| Bansic10 | 25 June–14 Jul 2010 | Urania | 13 | 700 | 26 | 4.086 | 0.230 | 0.166 | 0.462 | 4.606 | 0.299 | 14.155 | 0.017 | 38.742 | 0.0014 |
| Bansic11 | 08–26 Jul 2011 | Urania | 34 | 1130 | 65 | 5.400 | 0.254 | 0.135 | 0.425 | 4.860 | 0.348 | 14.196 | 0.010 | 38.753 | 0.0022 |
| Bansic12 | 04–23 Jul 2012 | Urania | 39 | 1711 | 68 | 4.407 | 0.244 | 0.170 | 0.342 | 4.443 | 0.342 | 14.336 | 0.016 | 38.814 | 0.0007 |
| Bansic13 | 26 June–16 Jul 2013 | Urania | 34 | 1700 | 65 | 4.473 | 0.216 | 0.163 | 0.338 | 4.623 | 0.271 | 14.325 | 0.017 | 38.819 | 0.0006 |
| Bansic14 | 22 Jul–9 Aug 2014 | Urania | 32 | 1700 | 61 | 4.753 | 0.190 | 0.178 | 0.299 | 4.047 | 0.305 | 14.474 | 0.022 | 38.852 | 0.0013 |
| Bansic15 | 16 Jul–3 Aug 2015 | Minerva Uno | 31 | 1700 | 57 | 2.976 | 0.402 | 0.148 | 0.476 | 2.589 | 0.528 | 14.677 | 0.020 | 38.858 | 0.0014 |
| Bansic16 | 30 June–14 Jul 2016 | Minerva Uno | 10 | 1700 | 23 | 4.002 | 0.277 | 0.096 | 0.585 | 3.097 | 0.416 | 14.794 | 0.022 | 38.892 | 0.0007 |
| Bansic17 | 13–29 June 2017 | Minerva Uno | 32 | 1700 | 52 | 4.017 | 0.290 | 0.167 | 0.397 | 4.193 | 0.294 | 14.705 | 0.021 | 38.900 | 0.0006 |
| Bansic18 | 07-19 Sept 2018 | G. Dallaporta | 16 | 700 | 16 | 4.460 | 0.142 | 0.095 | 0.520 | 4.223 | 0.185 | 14.584 | 0.018 | 38.885 | 0.0006 |
| Bansic19 | 30 Sept-12 Oct 2019 | G. Dallaporta | 6 | 72 | | | | | | | | | | | |
| Bansic20 | 16-25 Sept 2020 | G. Dallaporta | 11 | 1000 | 11 | 4.301 | 0.068 | 0.115 | 0.171 | 3.869 | 0.161 | 14.464 | 0.013 | 38.873 | 0.0006 |
| Bansic21 | 6-18 Sept 2021 | G. Dallaporta | 15 | 996 | 13 | 5.025 | 0.319 | 0.204 | 0.304 | 4.677 | 0.254 | 14.634 | 0.016 | 38.872 | 0.0005 |

| | | | | | | Layer 500-bottom | | | | | | | | | |
|---|---|---|---|---|---|---|---|---|---|---|---|---|---|---|---|
| Bansic10 | 25 June–14 Jul 2010 | Urania | 13 | 700 | 4 | 4.420 | 0.006 | 0.097 | 0.339 | 4.987 | 0.045 | 13.908 | 0.004 | 38.777 | 0.0002 |
| Bansic11 | 08–26 Jul 2011 | Urania | 34 | 1130 | 25 | 5.861 | 0.125 | 0.179 | 0.280 | 6.392 | 0.163 | 13.946 | 0.003 | 38.787 | 0.0002 |
| Bansic12 | 04–23 Jul 2012 | Urania | 39 | 1711 | 49 | 5.413 | 0.171 | 0.216 | 0.217 | 6.468 | 0.163 | 13.997 | 0.005 | 38.780 | 0.0003 |
| Bansic13 | 26 June–16 Jul 2013 | Urania | 34 | 1700 | 39 | 4.886 | 0.158 | 0.207 | 0.212 | 6.474 | 0.150 | 14.019 | 0.003 | 38.794 | 0.0002 |
| Bansic14 | 22 Jul–9 Aug 2014 | Urania | 32 | 1700 | 37 | 5.546 | 0.106 | 0.239 | 0.190 | 6.088 | 0.127 | 14.069 | 0.003 | 38.811 | 0.0003 |
| Bansic15 | 16 Jul–3 Aug 2015 | Minerva Uno | 31 | 1700 | 26 | 4.130 | 0.240 | 0.238 | 0.267 | 4.701 | 0.277 | 14.125 | 0.003 | 38.817 | 0.0003 |
| Bansic16 | 30 June–14 Jul 2016 | Minerva Uno | 10 | 1700 | 16 | 5.774 | 0.240 | 0.118 | 0.339 | 6.180 | 0.237 | 14.222 | 0.006 | 38.834 | 0.0005 |
| Bansic17 | 13–29 June 2017 | Minerva Uno | 32 | 1700 | 25 | 4.954 | 0.231 | 0.241 | 0.203 | 6.205 | 0.117 | 14.229 | 0.003 | 38.837 | 0.0003 |
| Bansic18 | 07-19 Sept 2018 | G. Dallaporta | 16 | 700 | 3 | 5.315 | 0.036 | 0.159 | 0.093 | 5.905 | 0.084 | 14.200 | 0.003 | 38.832 | 0.0003 |
| Bansic19 | 30 Sept-12 Oct 2019 | G. Dallaporta | 6 | 72 | | | | | | | | | | | |
| Bansic20 | 16-25 Sept 2020 | G. Dallaporta | 11 | 1000 | 7 | 4.650 | 0.017 | 0.155 | 0.070 | 5.038 | 0.030 | 14.201 | 0.003 | 38.834 | 0.0002 |
| Bansic21 | 6-18 Sept 2021 | G. Dallaporta | 15 | 996 | 7 | 5.474 | 0.299 | 0.241 | 0.279 | 6.229 | 0.191 | 14.248 | 0.003 | 38.815 | 0.0002 |

As far as the hydrological properties of the water masses in the study area, it is worth noting that over the (summer) period 2010-2021 in the surface layer the average temperature varied in the range 17.380-19.861 °C, with a general increasing trend peaking in 2020. Similarly, the salinity showed increasing values in the range 37.610-38.206 with a peak of in 2015 (Tab. 2). This layer is characterized by a strong interannual and spatial variability as subject to continuous interaction with the atmosphere, as also highlighted by one or two higher orders of magnitude in CV values of physical parameters in the superficial layer compared to the deeper layers (Fig. 2f, g; Tab. 2). Indeed, in the upper layer the CV of temperature varied between 0.148 (BANSIC10) and 0.240 (BANSIC15), and the CV of salinity ranged between 0.007 (BANSIC19) and 0.014 (BANSIC16).

Instead, the deeper water masses, with their lower variability in heat and salt content turn out to be much more suitable for monitoring any changes over long periods. In the IW layer the CV of temperature ranged between 0.010 (BANSIC11) and 0.022 (BANSIC14 and BANSIC16), while the CV of salinity ranged between 0.0005 (BANSIC21) and 0.0022 (BANSIC11) (Tab. 2). Values of temperature in our time series (2010-2021) shows an increase in average values of about 0.5 °C (14.155-14.634 °C), with a peak of 14.794 in 2017 (Tab. 2). Similarly, the corresponding increase in salinity was about 1.15 psu (37.742-38.885) with a peak of 38.900 psu reached in 2018 (Tab. 2). Similar trends have been also highlighted in the same area by Schroeder et al. (2017) and related to the increase to drying processes affecting the surface waters from which the IW originates. Within

13

the time series (2010-2021) two patterns can be distinguished, the first (2010-2016) is characterized by an average annual increase in temperature (dT/dt) of about 0.1 °C/year, the second one (2017-2020) by an annual decrease in temperature of 0.08 °C/year (Fig. 2i; Tab. 2). Finally, in 2021 a slight rise in temperature occurred (Fig. 2i; Tab. 2). Similarly, the salinity patterns show an average annual increase (dS/dt) of 0.022 over the period 2010-2016 and an annual decrease of 0.007 afterwards (2017-2021) (Fig. 2i; Tab. 2). A recent study advanced hypotheses on a possible link between the temperature and salinity positive trends over the period 2010-2016 and the anticyclonic phase of the NIG over the years 2006-2010, while the negative trends over the period 2017-2021 have been connected to the cyclonic phase of the NIG during years 2011-2016 (Placenti et al., 2022). Conversely, the nitrates and silicates mean annual concentrations show a slight decrease up to 2015-2016 and then slight increase until 2021 (Tab. 2), in agreement with the state of the art regarding the SC (Placenti et al., 2022).

The DW are characterized by very low values in CV of both temperature and salinity (between 0.003-0.006 and 0.002-0.005, respectively) with very slight differences across the yearly surveys (Tab. 2). Moreover, the average annual temperature and salinity slightly increased from 2010 until 2017 (13.908-14.299 °C and 38.777-38.837), and then slightly decreased until 2020 (Tab. 2). On the contrary, the patterns of nitrates and silicates would appear to be characterized by a slight decrease (5.861-4.130 and 6.392-4.701 µmol/l) between 2011 and 2015 and by a slight discontinuous increase afterwards until 2021 (Tab. 2).

**DATA AVAILABILITY**

**CONCLUSION**

The dataset described here has the advantage of having been collected within the same monitoring program implemented on an important area of the Mediterranean Sea. Over time, the data has been collected consistently by the same technicians and researchers, who have been able to apply a rigorous quality check during both field and laboratory activities. This made it possible to minimize any biases deriving from the different experience of the personnel and from the use of different types of instrumentation and protocols. The spatial and temporal variability that characterizes this dataset therefore reliably reflects the effect of environmental processes that occurred in the marine

329 environment, making this dataset usable for different fields of application. In support to this, the
330 analysis of the mean values and of the variability of the parameters along the water column and
331 among different surveys showed an agreement with the patterns commonly recognized in the
332 marine environment and highlighted in other datasets collected in different areas of the
333 Mediterranean Sea. Moreover, the analysis shown in this paper is highly consistent with the trends
334 evidenced in the literature concerning the Sicily Channel. In this framework, the availability of this
335 dataset to the scientific community fills an important lack in field observations of a crucial area, the
336 Sicily Channel, where exchanges between the western and eastern Mediterranean basin take place,
337 providing support to studies aimed at describing the ongoing processes as well as at realizing reliable
338 projections regarding the effects of these processes in the near future.

339

340 **AUTHOR CONTRIBUTIONS**

348

349 **COMPETING INTERESTS**

350 The authors declare that they have no conflict of interest.

351

352 **FINANCIAL SUPPORT**

361

**REFERENCES**

Belgacem, M., Chiggiato, J., Borghini, M., Pavoni, B., Cerrati, G., Acri, F., Cozzi, S., Ribotti, A., Álvarez, M., Lauvset, S. K., and Schroeder, K.: Dissolved inorganic nutrients in the western Mediterranean Sea (2004–2017), Earth Syst. Sci. Data, 12, 1985–2011, 2020, https://doi.org/10.5194/essd-12-1985-2020, 2020.

Ben Ismail, S., Schroeder, K., Sammari, C., Gasparini, G. P., Borghini, M., and Aleya, L.: Interannual variability of water mass properties in the Tunisia-Sicily Channel, J. Mar. Syst., 135, 14–28, 2014.

Bonanno, A., Placenti, F., Basilone, G., Mifsud, R., Genovese, S., Patti, B., Di Bitetto, M., Aronica, S., Barra, M., Giacalone, G., Ferreri, R., Fontana, I., Buscaino, G., Tranchida, G., Quinci E., and Mazzola, S.: Variability of water mass properties in the Strait of Sicily in summer period of 1998–2013, Ocean Sci.10:759–770, 2014.

Borghini, M., Bryden, H., Schroeder, K., Sparnocchia, S., and Vetrano, A.: The Mediterranean is becoming saltier, Ocean Sci. 10, 693–700, http://dx.doi.org/10.5194/os-10-693-2014, 2014.

Gačić, M., Schroeder, K., Civitarese, G., Cosoli, S., Vetrano, A., and Borzelli, G.L.E.: Salinity in the Sicily channel corroborates the role of the Adriatic-Ionian bimodal oscillating system (BiOS) in shaping the decadal variability of the Mediterranean overturning circulation, Ocean Sci. 9, 83–90, https://doi.org/10.5194/os-9-83-2013, 2013.

Gasparini, G.P., Ortona, A., Budillon, G., Astraldi, M., and Sansone, E.: The effect of the Eastern Mediterranean Transient on the hydrographic characteristics in the Strait of Sicily and in the Tyrrhenian Sea, Deep-Sea Res. I Oceanogr. Res. Pap. 52 (6), 915–935, 2005.

Grasshoff, K., Kremling, K., and Ehrhardt, M.: Methods of Seawater Analysis. Wiley-Vch Verlag, Weinheim, 1999.

Hansen, H. P. and Koroleff, F.: Determination of nutrients, Methods of Seawater Analysis, 10, 159–228, 1999.

Huertas, I.E., Rios, A.F., Garcia-Lafuente, J., Navarro, G., Makaoui, A., Sanchez-Roman, A., Rodriguez-Galvez, S., Orbi, A., Ruiz, J., and Perez, F.F.: Atlantic forcing of the Mediterranean oligotrophy, Glob. Biogeochem. Cycles 26, GB2022, http://dx.doi.org/10.1029/2011GB004167, 2012.

Krom, M.D., Woodward, E.M.S., Herut, B., Kress, N., Carbo, P., Mantoura, R.F.C., Spyres, G., Thingstad, T.F., Wassmann, P., Wexels Riser, C., Kitidis, V., Law, C.S., and Zodiatis, G.: Nutrient cycling in the south east Levantine basin of the Eastern Mediterranean: results from a phosphorus starved system, Deep-Sea Res. II 52 (22–23), 2879–2896, 2005.

Krom, M. D., Emeis, K. C., and Van Cappellen, P.: Why is the eastern Mediterranean phosphorus limited? Prog. Oceanogr., 85(3–4), 236–244, http://dx.doi.org/10.1016/j.pocean.2010.03.003, 2010.

Placenti, F., Schroeder, K., Bonanno, A., Zgozi, S., Sprovieri, M., Borghini, M, Rumolo, P., Cerrati, G., Bonomo, S., Genovese, S., Basilone, G., Haddoud, D. A., Patti, B., El Turki, A., Hamza, M., and Mazzola, S.: Water masses and nutrient distribution in the Gulf of Syrte and between Sicily and Libya, J. Marine Sys., 121–122, 36–46, 2013, http://dx.doi.org/10.1016/j.jmarsys.2013.03.012, 2013.

Placenti, F., Torri, M., Pessini, F., Patti, B., Tancredi, V., Cuttitta, A., Giaramita, L., Tranchida, G., and Sorgente, R.: Hydrological and biogeochemical patterns in the Sicily Channel: new insights from the last decade (2010-2020), Front. Mar. Sci. 9, https://doi.org/10.3389/fmars.2022.733540, 2022.

Placenti, F., Torri, M., Borghini, M., Cerrati, G., Cuttitta, A., Tancredi, V., Buscaino, C., and Patti, Bernardo. New hydrological-biogeochemical dataset (2010-2021) in the Strait of Sicily [Data set and metadata]. Zenodo. https://doi.org/10.5281/zenodo.8125006, 2023.

Powley, H.R., Krom, M.D., and Van Cappellen, P.: Understanding the unique biogeochemistry of the Mediterranean Sea: insights from a coupled phosphorus and nitrogen model Glob. Biogeochem. Cycles, 31, pp. 1010-1031, 10.1002/2017GB005648, 2017.

Redfield, A.C., Ketchum, B.H., and Richards, F.A.: The influence of organisms on the composition of sea water, In: Hill, M.N. (Ed.), The Sea, vol. 2. Interscience, New York, pp. 224–228, 1963.

Ribera D'Alcalà, M., Civitarese, G., Conversano, F., and Lavezza, R.: Nutrient ratios and fluxes hint at overlooked processes in the Mediterranean Sea, J. Geophys. Res.,108(C9),8106, doi:10.1029/2002JC0016500, 2003.

Roether, W., Manca, B.B., Klein, B., Bregant, D., Georgopoulos, D., Beitzel, V., Kovacević, V., and Luchetta, A.: Recent changes in eastern mediterranean deep waters, Science 271 (5247), 333–335, http://dx.doi.org/10.1126/science, 1996.

Schroeder, K., Gasparini, G. P., Borghini, M., Cerrati, G., and Delfanti, R.: Biogeochemical tracers and fluxes in the Western Mediterranean Sea, spring 2005, J. Mar. Syst. 80, 8–24, doi: 10.1016/j.jmarsys.2009.08.002, 2010.

Schroeder, K., Chiggiato, J., Josey, S. A., Borghini, M., Aracri, S., and Sparnocchia, S.: Rapid response to climate change in a marginal sea. Sci. Rep. 7:4065, doi: 10.1038/s41598-017-04455-5, 2017.

Schroeder, K., Chiggiato, J., Ben Ismail, S., Borghini, M., Patti, B. and Sparnocchia, S.: Mediterranean deep and intermediate water mass properties. In: Copernicus Marine Service Ocean State Report, Issue 3, Journal of Operational Oceanography, 12:sup1, s26–s30; doi: 10.1080/1755876X.2019.16330, 2019.

437    Sorgente, R., Olita, A., Oddo, P., Fazioli, L., and Ribotti, A.: Numerical simulation and decomposition
438        of kinetic energy in the Central Mediterranean: insight on mesoscale circulation and energy
439        conversion, Ocean Sci., 7, 503–519, doi: 10.5194/os-7-503-2011, 2011.

440    The Mermex group: Durrieu de Madron, X., Guieu, C., Sempéré, R., Conan, P., Cossa, D., D'Ortenzio,
441        F., Estournel, C., Gazeau, F., Rabouille, C., Stemmann, L., Bonnet, S.,Diaz, F., Koubbi, P.,
442        Radakovitch, O., Babin, M., Baklouti, M., Bancon-Montigny, C.,Belviso, S., Bensoussan, N.,
443        Bonsang, B., Bouloubassi, I., Brunet, C., Cadiou, J.-F.,Carlotti, F., Chami, M., Charmasson, S.,
444        Charrière, B., Dachs, J., Doxaran, D., Dutay,J.-C., Elbaz-Poulichet, F., Eléaume, M., Eyrolles, F.,
445        Fernandez, C., Fowler, S.,Francour, P., Gaertner, J.C., Galzin, R., Gasparini, S., Ghiglione, J.-F.,
446        Gonzalez, J.-L.,Goyet, C., Guidi, L., Guizien, K., Heimbürger, L.-E., Jacquet, S.H.M., Jeffrey,
447        W.H.,Joux, F., Le Hir, P., Leblanc, K., Lefèvre, D., Lejeusne, C., Lemé, R., Loÿe-Pilot, M.-
448        D.,Mallet, M., Méjanelle, L., Mélin, F., Mellon, C., Mérigot, B., Merle, P.-L., Migon, C.,Miller,
449        W.L., Mortier, L., Mostajir, B., Mousseau, L., Moutin, T., Para, J., Pérez, T.,Petrenko, A.,
450        Poggiale, J.-C., Prieur, L., Pujo-Pay, M., Pulido-Villena, Raimbault, P.,Rees, A.P., Ridame, C.,
451        Rontani, J.-F., Ruiz Pino, D., Sicre, M.A., Taillandier, V.,Tamburini, C., Tanaka, T., Taupier-
452        Letage, I., Tedetti, M., Testor, P., Thébault, H.,Thouvenin, B., Touratier, F., Tronczynski, J.,
453        Ulses, C., Van Wambeke, F.,Vantrepotte, V., Vaz, S., Verney, R.: Marine ecosystems'responses
454        to climatic and anthropogenic forcings in the Mediterranean, Prog. Oceanogr., 91.
455        doi:10.1016/j.pocean.2011.02.003.T, 2011.

456    SeaDataNet: Data Quality Control Procedures, 6th Framework of EC DG Research, Version 2.0, May
457        2010, https://www.seadatanet.org/Standards/Data-Quality-Control, 2010

458    Stansfield, K., Gasparini, G.P., and Smeed, D.A.: High-resolution observations of the path of the
459        overflow from the Sicily Strait, Deep Sea Res., Part I, 50, 1129–1149, 2003.

460    Van Cappellen, P., Powley, H. R., Emeis, K.-C., and Krom, M. D.: A biogeochemical model for
461        phosphorus and nitrogen cycling in the eastern Mediterranean Sea (EMS), Part 1. Model
462        development, initial conditions and sensitivity analyses, J. Mar. Syst., 139, 460–471, 2014.